Dual-function MR-guided hyperthermia

An innovative integrated approach and experimental demonstration of proof of principle

Sumser, Kemal; Bellizzi, Gennaro G.; Forner, Ria; Drizdal, Tomas; Hernandez Tamames, Juan A.; van Rhoon, Gerard C.; Paulides, Margarethus M.

DOI
10.1109/tbme.2020.3012734

Publication date
2021

Document Version
Final published version

Published in
IEEE Transactions on Biomedical Engineering

Citation (APA)
Sumser, K., Bellizzi, G. G., Forner, R., Drizdal, T., Hernandez Tamames, J. A., van Rhoon, G. C., & Paulides, M. M. (2021). Dual-function MR-guided hyperthermia: An innovative integrated approach and experimental demonstration of proof of principle. *IEEE Transactions on Biomedical Engineering*, *68*(2), 712-717. Article 9152076. https://doi.org/10.1109/tbme.2020.3012734

Dual-Function MR-guided Hyperthermia: An Innovative Integrated Approach and Experimental Demonstration of Proof of Principle

Kemal Sumser*, Gennaro G. Bellizzi* *Member, IEEE*, Ria Forner, Tomas Drizdal, Juan A. Hernandez Tamames, Gerard C. van Rhoon, Margarethus M. Paulides *Senior Member, IEEE*

***Abstract*—Temperature monitoring plays a central role in improving clinical effectiveness of adjuvant hyperthermia. The potential of magnetic resonance thermometry for treatment monitoring purposes led to several MR-guided hyperthermia approaches. However, the proposed solutions were sub-optimal due to technological and intrinsic limitations. These hamper achieving target conformal heating possibilities (applicator limitations) and accurate thermometry (inadequate signal-to-noise-ratio (SNR)). In this work, we studied proof of principle of a dual-function hyperthermia approach based on a coil array (64 MHz, 1.5 T) that is integrated in-between a phased array for heating (434 MHz) for maximum signal receive in order to improve thermometry accuracy. Hereto, we designed and fabricated a superficial hyperthermia mimicking planar array setup to study the most challenging interactions of generic phased-array setups in order to validate the integrated approach. Experiments demonstrated that the setup complies with the superficial hyperthermia guidelines for heating and is able to improve SNR at 2-4 cm depth by 17%, as compared to imaging using the body coil. Hence, the results showed the feasibility of our dual-function MR-guided hyperthermia approach as basis for the development of application specific setups.**

***Index Terms*—Hyperthermia; MR thermometry; MR-guided treatment; radiofrequency; phased array integration.**

I. Introduction

Typically, radiofrequency (RF) hyperthermia for cancer treatment consists of increasing the temperature of the tumor up to 40-44 °C , commonly using external electromagnetic field sources [1]. Given the demonstrated thermal dose-effect relations [2, 3], clinical effectiveness would benefit from achieving higher temperatures. Homogeneous and target conformal heating in the range of 41-43 °C for 30-60 minutes is currently considered optimal [4]. 3-Dimensional temperature monitoring is beneficial to enable real-time dosimetry and treatment guidance. Conventional dosimetry is currently pursued by invasive interstitial thermometry probes, providing limited spatial resolution [5]. Moreover, they are uncomfortable for the patient, time-consuming to set up and often unfeasible [6, 7]. Magnetic resonance (MR) thermometry has shown potential for 3D non-invasive temperature monitoring during hyperthermia [8, 9]. However, maximum signal-to-noise-ratio (SNR) in MR imaging is critically dependent on the distance of the receiver coils to the region of interest (ROI) [10, 11]. Also heating antennas need to be close to the ROI to minimize lengthy and energy absorbing paths of the RF waves through the tissues [12]. This motivated us to envision the next generation of a dual-function integrated approach to MR-guided hyperthermia enabling simultaneous close-to-ROI administration and monitoring of the thermal treatment. In this work, we aim to validate the feasibility of this novel approach.

A number of groups have proposed devices enabling MR thermometry guided hyperthermia treatment [11, 13-16]. However, many intrinsic pitfalls either limited the way to the clinic or their widespread adoption [17]. The first approach used a phased array of twelve dipole pairs working at 100 MHz for heating and relied on the scanner's body coil for MR imaging. Relying on the body coil as receiver yields to low SNR values and hence results in unpredictable MR thermometry accuracy levels [11, 17]. A more recent approach by Yeo et al., proposed the use of fast electronic switching to open or short-circuit capacitors [14]. In this way fast switching between C-type heating dipole antenna and MR coil mode was achieved for heating and imaging at 128 MHz (3 T). Another similar approach by Winter et al. used one single 298 MHz RF array for sequentially applying both heating and imaging at 7 T [13]. These latter two approaches allow to install receiver coils and heating antennas close to the patient skin, for achieving an improved imaging SNR level and good heating possibilities. However, these solutions not only require to switch between heating and imaging and imply using MRI scanners >3 T, they also restrict the heating frequency to the MR scanner's Larmor frequency. This limitation hampers to obtain optimal treatments as target conformal heating is only achieved within specific ranges of frequencies that are

Manuscript received in Jan. 2020.

* These authors contributed equally to this work.

This work was supported by the project KWF-11368 - "Multi-coil magnetic resonance guided hyperthermia for precision treatment of advanced head and neck carcinoma" and supported by COST Action MyWave CA17115 - "European network for advancing Electromagnetic hyperthermic medical technologies".

K. Sumser, G.G. Bellizzi, G.C. va Rhoon and M.M. Paulides is with Department of Radiation Oncology, University Medical Center Rotterdam, Erasmus MC – Cancer Institute, Rotterdam, The Netherlands (k.sumser@erasmusmc.nl)

R. Forner is with Department of Radiology, Utrecht Medical Center, Utrecht, The Netherlands

T. Drizdal is with Department of Biomedical Technology, Czech Technical University in Prague, Prague, Czech Republic

J.A. Hernandez Tamames is with Department of Radiology & Nuclear Medicine, University Medical Center Rotterdam, Erasmus MC, Rotterdam, The Netherlands

G.C. van Rhoon is also with Department of Applied Radiation and Isotopes, Reactor Institute Delft, Delft, The Netherlands

M.M. Paulides is also with Department of Electrical Engineering, Eindhoven University of Technology, Eindhoven, The Netherlands

This article has been accepted for publication in a future issue of this journal, but has not been fully edited. Content may change prior to final publication. Citation information: DOI 10.1109/TBME.2020.3012734, IEEE Transactions on Biomedical Engineering

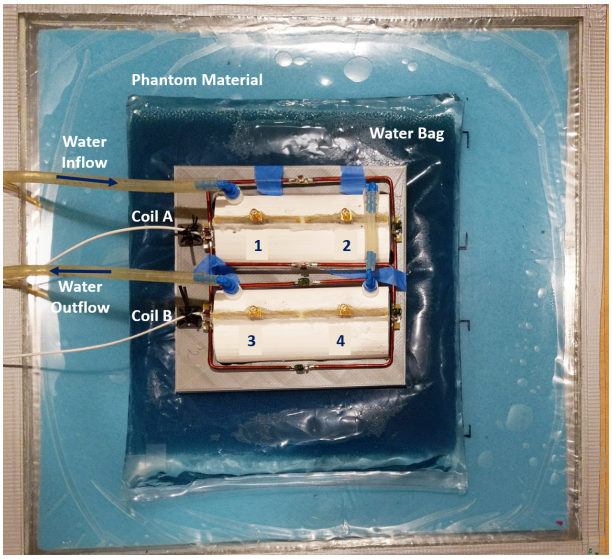

Fig. 1. Picture of the dual-function integrated RF system.

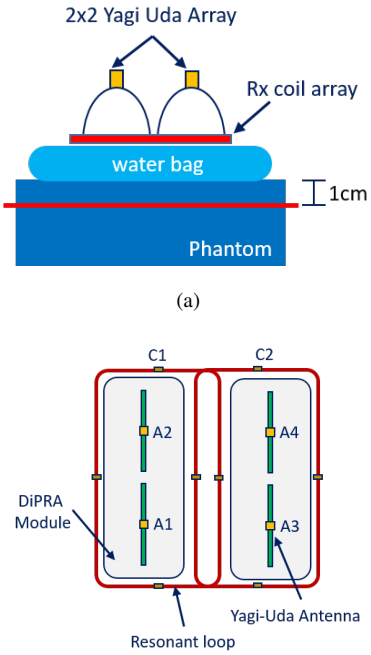

Fig. 2. Schematic cross section (a) and top view (b) of the dual-function integrated RF system.

different for each anatomical region [18]. As an example, the range of 400-600 MHz showed to enable optimal heating in the head and neck region [19-21]. Recently, Eigentler et al. [22] proposed a wideband antenna operating in the range of 400-600 MHz, while allowing imaging at 7 T. While this approach solves the problem of choosing the optimal heating frequency, it requires a complex and inefficient switching at high power when going from imaging to heating and ultrahigh field MR imaging, which limits the wide adaptation of MR-guided hyperthermia. In conclusion, a novel approach enabling an independent choice of the heating and imaging frequency is realistically needed for wide-scale adoption of MR-guided hyperthermia.

A possible solution would be an applicator integrating the two different functions, hence integrating two RF arrays: one for heating at 434 MHz and one for imaging at the MR scanner's Larmor frequency. Through integration, firstly, operating frequencies can be independently chosen allowing to use commercially available MR scanner without compromising on heating quality. Secondly, higher SNR levels needed for accurate MR thermometry would be achieved as the integrated system would stand in the skin proximity. Ideally an integrated system will consist of a heating device leaving sufficient space to integrate local imaging coils where both devices are non- or minimally interfering each other's proper operation. In a first attempt, Paulides et al showed feasibility of applying hyperthermia with 12 patch antennas operating at 434 MHz in a 1.5 T GE 450w MR scanner using the body coil for imaging [23]. However, the patch antennas caused shadowing in the MR-image resulting in poor SNR. This motivated us to design of an innovative Yagi-Uda antenna concept to minimize influence of the hyperthermia antennas on MR compatibility [17].

Therefore, the purpose of this study was to experimentally investigate the feasibility of heating at 434 MHz and imaging at 64 MHz (1.5 T) using an integrated dual-function RF array 1) to identify the needs for clinical systems and 2) to pave the way for application specific phased-array systems design (such as head and neck, breast, etc). A dedicated experimental setup has been manufactured integrating a 2-channel receiver-only coil array for MR imaging at 64 MHz (1.5 T, proton) into a 4-channel heating array at 434 MHz. The scattering parameters of the integrated systems has been characterized by means of a vector network analyzer (VNA). Our aim is to show proof of principle for phased array systems, however this experimental setup resembles a superficial hyperthermia setup. Therefore, we investigated heating performance using the guidelines for superficial hyperthermia [12]. Imaging performances have been investigated in a setup mimicking the final application setup and using the integrated body coil of the 1.5 T MRI-scanner for comparison.

II. Materials and Methods

A. Dual-Function Integrated Experimental System

1) MR Receiver Coil Array: Design and Compliance Tests: The dedicated coil array is a two-channel receive-only array and consists of two identical rectangular shaped loops (15×8 cm) fabricated as a combination of etched copper wire (0.3 cm diameter) and of copper printed circuit boards (PCBs) with capacitor breaks (trace width of 0.4cm produced by Eurocircuits Gmbh, Belgium). Coils have been tuned and matched when placed on a 2 cm thick deionized water bolus, which was placed on top of a muscle-equivalent phantom having an electrical conductivity of 0.91 S/m and a relative permittivity of 63 at 64 MHz.

The loops were tuned to 63.89 MHz using four tuning capacitors (3×68 pF and 1×56 pF, ATC multi-layer ceramic 100B/TN series) with an additional matching network (2×51

pF, ATC multi-layer ceramic 100B/TN series) at the feed port to achieve 50 Ohm. The loops are connected to a 10 cm (Habia RG174 (50 Ohm, silver-plated copper & copper) coaxial cable at the feed port. The distance between the segmenting capacitors was determined by optimizing the tradeoff between coil load sensitivity and high resistive losses. Further, to minimize coupling between elements in the array, geometric overlap was used to achieve next-neighbor decoupling.

Receive loops were decoupled from the transmit MR body coil by means of both an active and a passive diode detuning circuit. Both circuits were implemented by placing the diode (Macom MA4P7461F-1072T and Microsemi UMX9989AP) in parallel with tuning capacitor to achieve adequate decoupling level. When loaded with the phantom, the detuning performance of the tuned and matched was quantified by switching the diode on and off by means of an external power supply and measuring the S_{21} between the two states.

The noise correlation matrix has been measured to investigate the decoupling level between the two resonant loops. Local static magnetic field artifacts have been investigated by measuring the B0 map in presence and absence of the coil using the body coil with a spoiled RF Gradient Echo (TR = 50 ms, Flip Angle = 15°, Image Matrix = 256×256, Read out Bandwidth = 31.25 kHz, FOV = 25.6 cm, Slice thickness = 0.1 cm). Finally, the proper functioning of the detuning circuits has been investigated by measuring the B1 map in presence and absence of the coil using the body coil applying a Bloch-Siegert Shift (TR = 28 ms, TE = 12.4 ms, Flip Angle = 15°, Image Matrix = 128×128, Read out Bandwidth = 31.25 kHz, FOV = 25.6 cm, Slice thickness = 0.1 cm) [22].

2) Hyperthermia Heating Phased Array: The heating array is made up by two dielectric parabolic reflector antenna modules filed with deionized water for reduction of the antenna geometrical dimensions as proposed in [7]. These modules are tailored antenna encasings with a parabolic back shape and they were designed to reduce the amount of water needed, minimize the cross-coupling, regain focusing and to allow integration of MR surface receive coil. Sizing of each module was engineered to optimize the antenna's reflection and cross-coupling characteristics. The two modules were positioned at 2 cm distance. Each of these modules contains two Yagi-Uda antennas for which heating performance and MR compatibility were verified in a previous study [25]. The two modules were filled with deionized water.

B. Experimental Setup

A tailored experimental setup was built to demonstrate both heating and imaging capabilities of the dual function hyperthermia applicator in combination with a 1.5 T MRI.

1) Characterization of the Integrated RF System: Characterization of the integrated system is needed to investigate feasibility of simultaneous operation of the devised approach. To this end, the scattering matrix of both the heating array (434 MHz) and the coil array (63.89 MHz) for MR imaging was measured. Finally, the transmission coefficient (S_{21}) between the two RF systems has been measured to assess feasibility of simultaneous operation [11]. A calibrated (Rohde&Schwarz, ZNC3) VNA was used to perform all measurements.

2) Heating Experiments: Figures 1 and 2 show a picture and a schematic representation of the setup used for evaluating the heating performances. It aims at mimicking the clinical application setup in which a water bolus is placed between the patient skin and the dual function applicator. This is used to enhance the electromagnetic coupling and to remove skin heating. The dual function applicator has a surface area of 15×15 cm^2. As illustrated in Figure 2 (a), the coil array was centered on top of a 2 cm thick sealed back representing the water bolus (30×30×2 cm^3) containing deionized water and a plastic sponge for structural support. According to superficial hyperthermia guidelines [12], a 7 cm thick muscle-equivalent phantom (dimensions: (47×47×7 cm^3)) was prepared with a mix of deionized water, agar, sodium chloride, polyethylene powder and TX-151, having electrical conductivity 0.98 S/m and relative permittivity 68 at 434 MHz, thermal conductivity 0.6 W/m/C, specific heat 3800 W/kg/C. The dielectric properties were measured with an open-ended coaxial probe DAK-12 (v2.4 SPEAG) connected to a Rohde & Schwarz ZNC3 vector network analyzer and the thermal properties were measured with a TEMPOS thermal property analyzer, equipped with SH-3 sensor (METER Group AG, Munchen, Germany).

The water boluses were designed according to ESHO guidelines [12] ensuring both an optimal contact area with the phantom and extension beyond the radiating aperture. According to the guidelines, water bags were fabricated to have a planar dimension larger than the heating area (15×15 cm^2). In this work, we kept the water bolus at room temperature of approximately 25 °C. Although water temperature plays a central role, in this work we aimed at demonstrating the dual-functioning of our approach more than optimizing the clinical application of a superficial applicator.

Heating performance have been assessed according to [12]. However, in this work we do not aim at demonstrating the feasibility of a superficial applicator. The temperature rise (TR) and the thermal effective field size (TEFS) have been measured using 180 W total forward power for 4 minutes. The TEFS is defined as the area within the 50% of maximum TR contour in the 1 cm deep plane under the aperture. To this end, we used the described layered muscle-equivalent phantom and an infrared (IR) camera to measure the temperature distribution on the 1cm-deep-layer.

Finally, we modelled the experimental setup in Sim4Life (v.5.2.0, Zurich MedTech, Zurich, Switzerland). A 433.92 MHz harmonic excitation signal was applied to each antenna. 20 periods were simulated to ensure steady state of all signals. The size of the calculation domain was 11.6 million voxels, with a maximum voxels size of 2×2×2 mm^3). Transient 3D temperature distributions were calculated using the thermal solver in Sim4Life (1 mm uniform grid). The measured dielectric and thermal properties of the phantom were used in the simulations. The initial temperature in the phantom was set to 25 °C and mixed boundary conditions were applied to the phantom – background interface (heat transfer coefficients h = 8 W/m^2/°C, and outside temperature T = 25 °C).

3) MR Imaging Experiments: The experimental setup used for MR imaging experiments is similar to the one described in the section on heating experiments. However, receiver coils

This article has been accepted for publication in a future issue of this journal, but has not been fully edited. Content may change prior to final publication. Citation information: DOI 10.1109/TBME.2020.3012734, IEEE Transactions on Biomedical Engineering

TABLE I
MEASURED COUPLING BETWEEN THE HEATING ANTENNA ELEMENTS AND THE RECEIVER COILS AT 434 MHZ.

	A1	A2	A3	A4	C1	C2
A1	-18.0	-37.4	-30.7	-30.9	-48.5	-59.1
A2	-37.4	-19.6	-29.8	-29.9	-57.0	-58.0
A3	-30.7	-29.8	-19.4	-26.3	-57.5	-52.7
A4	-30.9	-29.9	-26.3	-22.9	-63.4	-54.9

are placed on top of the water bolus which is positioned on top of a calibration phantom (CTL Lower TL, P/N U1-150027, GE Medical Systems - MR Division, Waukesha, WI) provided by the MR vendor with T1 of 108 ms and T2 of 96 ms. The SNR was measured using three region of interest (ROI) centered at 3, 6 and 9 cm in this phantom. This investigation has been carried out using water boluses having 2, 4 and 6 cm thicknesses mimicking the clinical scenarios, to assess its effect on image quality. Performances have been benchmarked to the body coil of a GE (General Electric Healthcare, Milwaukee, WI) 450W 1.5 T scanner. A Spoiled Gradient Echo sequence has been used with the following parameters: Flip angle = 21°, FOV = 50 cm, TE = 4.5 ms, TR = 100 ms, and 0.2 cm voxel size.

III. RESULTS

A. Characterization of the Integrated System

Measurement of the scattering matrix for the heating 4-element phased array, operating at 434 MHz, shown a reflection coefficient equal to -20±2 dB and a cross-coupling equal to -31±2 dB. The decoupling between the two RF arrays has been measured at the heating frequency, i.e., 434 MHz, and it is equal to -56±4 dB. The measured reflection coefficient of the Rx-only coil array was -21±1 dB whereas a decoupling of -12 dB has been achieved through geometric overlap of 1.1 cm. The loops have on average an unloaded quality factor of ≈250 and a loaded of ≈30 giving an adequate ratio according to [26]. The noise correlation matrix identified a decoupling level <0.1 between the two resonant loops. Absence of local static magnetic field artifacts has been assessed. The comparison of the two B1 maps, visualized in Figure 3, performed in the presence and absence of the receive array show a deviation of less than 4% proving the proper functioning of the coil array.

B. Heating Experiments

Figure 4 depicts the simulated and experimental temperature rise map and the corresponding TEFS map achieved when using 180 W forward power for 4 minutes. The numerical model predicted two heat focuses below the antenna modules with the left one smaller than the right one. The measured temperature increase maps shown in the middle figure of Figure 4 show qualitative agreement. The measurements appear to be in agreement with the simulations (R^2 = 0.68) except for the higher predicted temperature increases at the edges of the phantom. We allocate this mismatch to a mismatch in antenna phases and boundary conditions set for the numerical model. The maximum temperature achieved is +8.6 °C which fulfills the ESHO requirements of 6 °C temperature increase in six minutes [12]. The TEFS map has been drawn according to [12] with the reference temperature TR at 4.3 °C. Results indicate no imprints nor preferential heating caused by the coil that surrounds the antenna cavities.

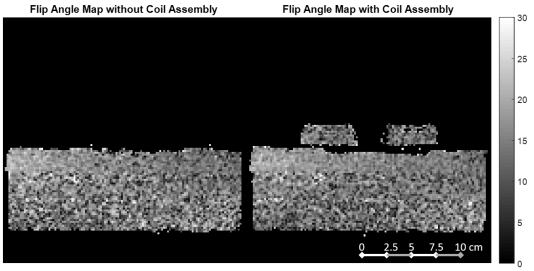

Fig. 3. Flip angle maps acquired in absence and presence of the dual function applicator

C. MR Imaging Experiments

Figure 5 depicts the magnitude images acquired when using either the integrated 2-channel coil or the body coil as receiver. The case of a 2, 4 and 6 cm thick water bolus was investigated and images for each case are reported. Figure 6 reports the SNR values achieved using three ROI centered at increasing depth from the phantom surface. Results show that the SNR levels achieved using the integrated 2-channel coil are always better than the one achieved using the body coil for any studied thickness of the water bolus. However, as expected, SNR worsens with increasing thickness of the water boluses. At an average depth of 3 cm from the phantom surface, i.e., within ROI 1, a 6 cm thick water bolus worsens the SNR by -8% when compared to a 2 cm thick one. Hence, our results show 2 cm thick water bolus is preferable for the application. In this case, the integrated 2-channel coil achieves an average SNR increase of +17% within ROI 1 (2-4 cm in tissue), when compared to the body coil.

IV. DISCUSSION

The results of our investigation experimentally validate the feasibility of our innovative approach to MR-guided hyperthermia, which enables truly simultaneous dual-function operation. The reduced scale setup indicates a minimal system's interaction (-56 dB) between the two RF arrays and suitability for proper functioning both in heating and imaging modality. Our results demonstrate a SNR improvement (+17%) when using close-to-skin receiver MR coils instead of the body coils and heating performances compliant with the superficial hyperthermia guidelines [12]. The results of this paper pave the way of the development of the next generation dual-function integrated approach to MR-guided head and neck hyperthermia systems.

In their pioneering work [11], Gellermann et al. identified that one of the main issues related to MR-guided hyperthermia is the electromagnetic compatibility problem of interference between the MR scanner and the hyperthermia RF applicator.

This article has been accepted for publication in a future issue of this journal, but has not been fully edited. Content may change prior to final publication. Citation information: DOI 10.1109/TBME.2020.3012734, IEEE Transactions on Biomedical Engineering

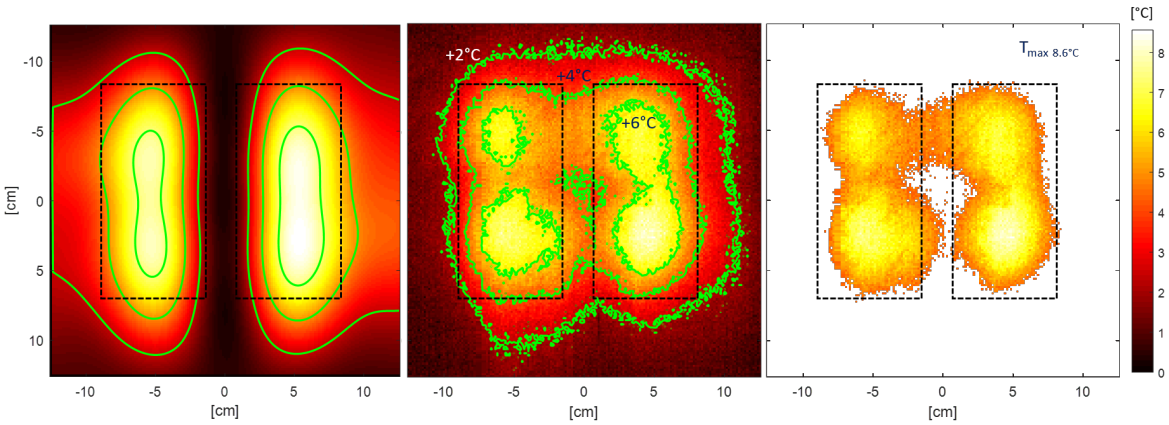

Fig. 4. (left) Simulated temperature rise map achieved when using 180 W forward power for 4 minutes. (middle) Measured temperature rise map achieved when using 180 W forward power for 4 minutes. (right) Corresponding TEFS map using Tmax equal to 8.6 °C. Antenna cavities shape prediction is overlapped in dashed black lines.

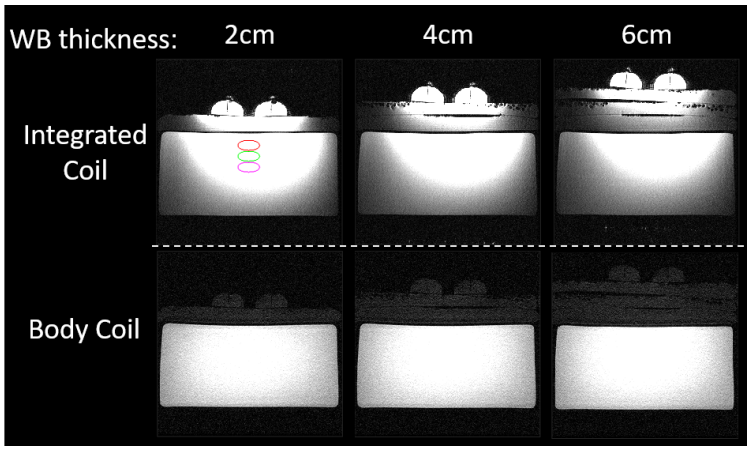

Fig. 5. Comparison of magnitude images acquired using either the integrated 2-channel coil or the body coil as receiver, when using a 2, 4, and 6 cm thick water boluses. Three ROIs are centered at 3, 6 and 9 cm within the phantom surface and are marked in red, green and magenta, respectively.

The first is generally able to receive and analyze low-power signals of μW at its operating frequency, whereas the second aims at transmitting power signals at therapeutic levels of kW (~2 kW) at a different frequency. They identified the heating signal must be attenuated by -125 dB in the receiving path of the MR scanner. In this framework, the low coupling level between the two RF systems is a crucial feature yielding to simultaneous dual-function operation. The sensibly low coupling (-56 dB) achieved by our approach results from a properly engineering design where geometrical (orthogonal) decoupling of the heating antennas from the imaging coils is pursued [27]. Furthermore, for head and neck hyperthermia, power signals at therapeutic levels do not exceed 300 W. Therefore, in case of more strict requirements, a dedicated RF filter with -60 dB has to be embedded in the MR scanner instead of -105 dB one as proposed in [11].

With this work, we aimed to experimentally validate the feasibility of heating and imaging via an integrated RF array. Investigating both imaging and heating capabilities, we evaluated whether any undesired interaction occurs between the two systems [11]. Also in HIFU devices coils have been integrated for signal receive closer to the target to improve MRT [28, 29]. This showed to greatly improve image quality. However, please not that HIFU systems are by definition much better decoupled since these do not exploit electromagnetic waves that interfere with those of the MR scanner. Accordingly, the measured SNR increase when coils are closer to the skin is consistent with the predictions and it suggests the need for a thin waterbolus (<2 cm) towards achieving such SNR levels. When assuming that the temperature-to-noise ratio is proportional to SNR [30], we expect a reduction in the temperature standard deviation of 180% at 2 cm depth from the surface and 31% at 6 cm depth from the surface. Note that these values are theoretical, the actual improvement depends on factors such like motion in and near the region of interest, scanner field drift etc. Besides, the measured heating pattern achieved using the fabricated experimental setup resembles the one achieved in the simulation-guided design phase [25], and there is no interference (e.g., preferred heating paths or distortions) due to the presence of the coil array. Finally, it is noteworthy to stress that such a heating pattern is achieved with an integrated system that was not properly designed and engineered for superficial heating. Although our study shows the proof of principle of coils integrated in an RF

This article has been accepted for publication in a future issue of this journal, but has not been fully edited. Content may change prior to final publication. Citation information: DOI 10.1109/TBME.2020.3012734, IEEE Transactions on Biomedical Engineering

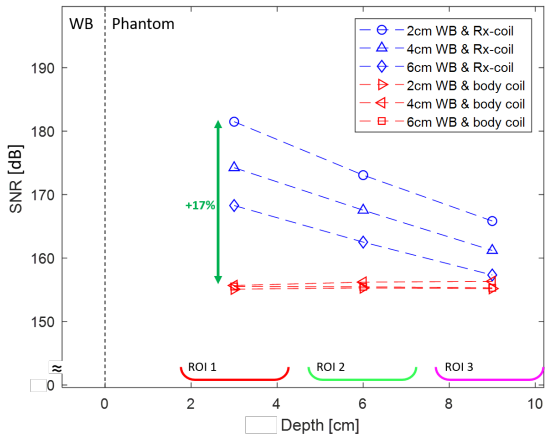

Fig. 6. Comparison of the SNR levels achieved when using the proposed integrated system or the body coil for increasing depth in the phantom, respectively, ROI 1, 2 and 3.

hyperthermia device, the setup currently is not optimized with superficial hyperthermia in mind. Since the setup did resemble this application, we used the clear and concise guidelines that exist for this application in our validation [12]. Simultaneously, this setup also covers the most challenging interactions, i.e. those between neighboring elements, of a phased array setup [31]. Hence, for both applications, this study provides a very solid proof of principle.

V. Conclusion

In this work, we proposed and experimentally demonstrated the feasibility of an innovative dual-function approach to MR-guided hyperthermia. Our approach is based on a close-to-body integrated system which includes a phased array for optimal heating and a coil array for accurate thermometry. This allows to optimally and independently pick the operating frequencies for heating and imaging without any compromise. Our results show the feasibility of the dual-function MR-guided hyperthermia approach and will pave the way for its development and clinical implementation.

References

[1] Stauffer, P.R., Evolving technology for thermal therapy of cancer. International Journal of Hyperthermia, 2005. 21(8): p. 731-744.
[2] Sherar, M., et al., Relationship between thermal dose and outcome in thermoradiotherapy treatments for superficial recurrences of breast cancer: data from a phase III trial. International Journal of Radiation Oncology* Biology* Physics, 1997. 39(2): p. 371-380.
[3] Franckena, M., et al., Hyperthermia dose-effect relationship in 420 patients with cervical cancer treated with combined radiotherapy and hyperthermia. European Journal of Cancer, 2009. 45(11): p. 1969-1978.
[4] van den Tempel, N., et al., The effect of thermal dose on hyperthermia-mediated inhibition of DNA repair through homologous recombination. Oncotarget, 2017. 8(27): p. 44593.
[5] Paulides, M.M., G.M. Verduijn, and N. Van Holthe, Status quo and directions in deep head and neck hyperthermia. Radiation Oncology, 2016. 11(1): p. 21.
[6] van der Zee, J., et al., Practical limitations of interstitial thermometry during deep hyperthermia. International Journal of Radiation Oncology* Biology* Physics, 1998. 40(5): p. 1205-1212.
[7] Curto, S., et al., Quantitative, Multi-institutional Evaluation of MR Thermometry Accuracy for Deep-Pelvic MR-Hyperthermia Systems Operating in Multi-vendor MR-systems Using a New Anthropomorphic Phantom. Cancers, 2019. 11(11): p. 1709.
[8] Winter, L., et al., Magnetic resonance thermometry: methodology, pitfalls and practical solutions. International Journal of Hyperthermia, 2016. 32(1): p. 63-75.
[9] Paulides, M.M., et al. Feasibility of MRI-guided hyperthermia treatment of head and neck cancer. in The 8th European Conference on Antennas and Propagation (EuCAP 2014). 2014. IEEE.
[10] Kulkarni, M.V., J.A. Patton, and R.R. Price, Technical considerations for the use of surface coils in MRI. American Journal of Roentgenology, 1986. 147(2): p. 373-378.
[11] Gellermann, J., et al., A practical approach to thermography in a hyperthermia/magnetic resonance hybrid system: Validation in a heterogeneous phantom. International Journal of Radiation Oncology* Biology* Physics, 2005. 61(1): p. 267-277.
[12] Dobšíček, H.T., et al., Quality assurance guidelines for superficial hyperthermia clinical trials: II. Technical requirements for heating devices. Strahlentherapie und Onkologie: Organ der Deutschen Rontgengesellschaft...[et al], 2017. 193(5): p. 351-366.
[13] Winter, L., et al., Design and evaluation of a hybrid radiofrequency applicator for magnetic resonance imaging and RF induced hyperthermia: electromagnetic field simulations up to 14.0 Tesla and proof-of-concept at 7.0 Tesla. PloS one, 2013. 8(4): p. e61661.
[14] Yeo, D., et al., Investigation of a dual-function applicator for RF hyperthermia and MRI. Proc of Inter Soc for Magn Reson in Med (ISMRM), 2011.
[15] Weihrauch, M., et al., Adaptation of antenna profiles for control of MR guided hyperthermia (HT) in a hybrid MR-HT system. Medical physics, 2007. 34(12): p. 4717-4725.
[16] Adibzadeh, F., et al., Systematic review of pre-clinical and clinical devices for magnetic resonance-guided radiofrequency hyperthermia. International Journal of Hyperthermia, 2020. 37(1): p. 15-27.
[17] Samulski, T.V., et al., Application of new technology in clinical hyperthermia. International journal of hyperthermia, 1994. 10(3): p. 389-394.
[18] Bellizzi, G.G., et al., Predictive value of SAR based quality indicators for head and neck hyperthermia treatment quality. International Journal of Hyperthermia, 2019. 36(1): p. 456-465.
[19] Paulides, M.M., et al., Theoretical investigation into the feasibility to deposit RF energy centrally in the head-and-neck region. International Journal of Radiation Oncology* Biology* Physics, 2005. 63(2): p. 634-642.
[20] Guérin, B., et al., Computation of ultimate SAR amplification factors for radiofrequency hyperthermia in non-uniform body models: impact of frequency and tumour location. International Journal of Hyperthermia, 2018. 34(1): p. 87-100.
[21] Schooneveldt, G., et al., Hyperthermia treatment planning including convective flow in cerebrospinal fluid for brain tumour hyperthermia treatment using a novel dedicated paediatric brain applicator. Cancers, 2019. 11(8): p. 1183.
[22] Eigentler, T.W., et al., Wideband Self-Grounded Bow-Tie Antenna for Thermal MR. NMR in Biomedicine, 2020.
[23] Paulides, M.M., et al., Laboratory prototype for experimental validation of MR-guided radiofrequency head and neck hyperthermia. Physics in Medicine & Biology, 2014. 59(9): p. 2139.
[24] Sacolick, L.I., et al., B1 mapping by Bloch-Siegert shift. Magnetic resonance in medicine, 2010. 63(5): p. 1315-1322.
[25] Paulides, M.M., et al., Novel applicator design for MR guided RF hyperthermia in head and neck cancers: heating performance and RF coupling, in SMRT, 27th Annual Meeting Joint ISMRM and ESMRMB. 2018.
[26] Hoffmann, J., et al., Safety testing and operational procedures for self-developed radiofrequency coils. NMR in Biomedicine, 2016. 29(9): p. 1131-1144.
[27] Paulides, M.M., et al., A printed Yagi–Uda antenna for application in magnetic resonance thermometry guided microwave hyperthermia applicators. Physics in Medicine & Biology, 2017. 62(5): p. 1831.
[28] Minalga, E., et al., An 11-channel radio frequency phased array coil for magnetic resonance guided high-intensity focused ultrasound of the breast. Magnetic Resonance in Medicine, 2013. 69(1): p. 295-302.
[29] Deckers, R., et al., Performance analysis of a dedicated breast MR-HIFU system for tumor ablation in breast cancer patients. Physics in Medicine & Biology, 2015. 60(14): p. 5527.
[30] Rieke, V. and K.B. Pauly, Journal of Magnetic Resonance Imaging: JMRI. J Magn Reson Imaging, 2008. 27(2): p. 376-390.
[31] Paulides, M.M., et al., A head and neck hyperthermia applicator: Theoretical antenna array design. International Journal of Hyperthermia, 2007. 23(1): p. 59-67.